J|A|C|S
ARTICLES
Published on Web 04/18/2003

Adsorption of CF_4 on the Internal and External Surfaces of Opened Single-Walled Carbon Nanotubes: A Vibrational Spectroscopy Study

Oleg Byl,[†] Petro Kondratyuk,[†] Scott T. Forth,[‡] Stephen A. FitzGerald,[‡] Liang Chen,[§] J. Karl Johnson,[§] and John T. Yates, Jr.*[,†]

Contribution from the Department of Chemistry, Surface Science Center, University of Pittsburgh, Pittsburgh, Pennsylvania 15260, Department of Chemical and Petroleum Engineering, University of Pittsburgh, Pittsburgh, Pennsylvania 15261, National Energy Technology Laboratory, Pittsburgh, Pennsylvania 15236, and Department of Physics, Oberlin College, Oberlin, Ohio 44074

Received July 11, 2002; E-mail: jyates@pitt.edu

Abstract: Infrared spectroscopy has been used to make the first experimental discrimination between molecules bound by physisorption on the exterior surface of carbon single-walled nanotubes (SWNTs) and molecules bound in the interior. In addition, the selective displacement of the internally bound molecules has been observed as a second adsorbate is added. SWNTs were opened by oxidative treatment with O_3 at room temperature, followed by heating in a vacuum to 873 K. It was found that, at 133 K and 0.033 Torr, CF_4 adsorbs on closed SWNTs, exhibiting its ν_3 asymmetric stretching mode at 1267 cm^{-1} (red shift relative to the gas phase, 15 cm^{-1}). Adsorption on the nanotube exterior is accompanied by adsorption in the interior in the case of opened SWNTs. Internally bound CF_4 exhibits its ν_3 mode at 1247 cm^{-1} (red shift relative to the gas phase, 35 cm^{-1}). It was shown that, at 133 K, Xe preferentially displaces internally bound CF_4 species, and this counterintuitive observation was confirmed by molecular simulations. The confinement of CF_4 inside (10,10) single-walled carbon nanotubes does not result in the production of lattice modes that are observed in large 3D ensembles of CF_4.

I. Introduction

Since the discovery of single-walled carbon nanotubes (SWNTs) by Iijima[1] and by Bethune et al.[2] in 1993, there has been a large interest in their application as sorbents.[3−10] This is due to the deep potential energy well for adsorption in the interior of the nanotube.[11−13] The synthesis of SWNTs normally produces closed structures where each tube is terminated by an end cap, which prevents adsorption within the interior.[14,15] Oxidative chemical treatments[16,17] must be applied to the closed SWNTs to open the end caps to access the interior of the nanotubes.[18] While oxidation in solution [$HNO_3 + H_2O_2 + H_2SO_4$] has been found to be effective for opening closed SWNTs, we have developed a gas-phase ozone oxidation process, which is more easily controlled. This O_3 oxidation procedure has been extensively investigated by IR spectroscopy in previous studies.[19,20] Oxidation can remove the end caps of individual SWNTs as well as produce or enlarge vacancy defects on the nanotube walls. Both carbonyl groups and C−O−C functional groups are known to form at the rims and at defective wall sites by oxidation.[18,19,21] Heating to 773−1073 K removes these blocking groups (by evolution of CO and CO_2[22]), leaving open entry ports for gas adsorption into the interior.[23]

* To whom correspondence should be addressed.
[†] Surface Science Center, University of Pittsburgh.
[‡] Oberlin College.
[§] Department of Chemical and Petroleum Engineering, University of Pittsburgh, and National Energy Technology Laboratory.

(1) Iijima, S.; Ichihashi, T. *Nature* **1993**, *363*, 603.
(2) Bethune, D. S.; Kiang, C. H.; de Vries, M. S.; Gorman, G.; Savoy, R.; Vazquez, J.; Beyers, R. *Nature* **1993**, *363*, 605.
(3) Muris, M.; Dupont-Pavlovsky, N.; Beinfait, M.; Zeppenfeld, P. *Surf. Sci.* **2001**, *492*, 67.
(4) Eswaramoorthy, M.; Sen, R.; Rao, C. N. R. *Chem. Phys. Lett.* **1999**, *304*, 207.
(5) Fujiwara, A.; Ishii, K.; Seumatsu, H.; Kataura, H.; Maniwa, Y.; Suzuki, S.; Achiba, Y. *Chem. Phys. Lett.* **2001**, *336*, 205.
(6) Talapatra, S.; Zambano, A. Z.; Weber, S. E. *Phys. Rev. Lett.* **2000**, *85* (1), 138.
(7) Talapatra, S.; Migone, A. D. *Phys. Rev. Lett.* **2001**, *87* (20), 206106.
(8) Long, R. Q.; Yang, R. T. *Ind. Eng. Chem. Res.* **2001**, *40*, 4288.
(9) Muris, M.; Dufau, N.; Bienfait, M.; Dupont-Pavlovsky, N.; Grillet, Y.; Palmari, J. P. *Langmuir* **2000**, *16*, 7019.
(10) Weber, S. E.; Talapatra, S.; Journet, C.; Zambano, A.; Migone, A. D. *Phys. Rev. B* **2000**, *61*, 13150.
(11) Simonyan, V. V.; Johnson, J. K.; Kuznetsova, A.; Yates, J. T., Jr. *J. Chem. Phys.* **2001**, *114*, 4180.
(12) Stan, G.; Cole, M. W. *Surf. Sci.* **1998**, *395*, 280.
(13) Duren, T.; Keil, F. J. *Chem. Eng. Technol.* **2001**, *24*, 698.
(14) *Carbon Nanotubes: preparation and properties*; Ebbsen, T. W., Ed.; CRC Press: Boca Raton, FL, 1997.
(15) *Science of Fullerenes and Carbon Nanotubes*; Dresselhaus, M. S., Dresselhaus, G., Eklund, P. C., Eds.; Academic Press: New York, 1996.
(16) Zimmerman, J. L.; Bradley, R. K.; Huffman, C. B.; Hauge, R. H.; Margrave, J. L. *Chem. Mater.* **2000**, *12*, 1361.
(17) Mawhinney, D. B.; Naumenko, V.; Kuznetsova, A.; Yates, J. T., Jr.; Liu, J.; Smalley, R. E. *Chem. Phys. Lett.* **2000**, *324*, 213.
(18) Kuznetsova, A.; Mawhinney, D. B.; Naumenko, V.; Yates, J. T., Jr.; Liu, J.; Smalley, R. E. *Chem. Phys. Lett.* **2000**, *321*, 292.
(19) Mawhinney, D. B.; Naumenko, V.; Kuznetsova, A.; Yates, J. T., Jr.; Liu, J.; Smalley, R. E. *J. Am. Chem. Soc.* **2000**, *122*, 2383.
(20) Mawhinney, D. B.; Yates, J. T., Jr. *Carbon* **2001**, *39*, 1167.
(21) Kuznetsova, A.; Popova, I.; Yates, J. T., Jr.; Bronikowski, M. J.; Huffman, C. B.; Liu, J. Smalley, R. E.; Hwu, H. H.; Chen, J. G. *J. Am. Chem. Soc.* **2001**, *123*, 10699.

Adsorption in the interior of a nanotube may also be accompanied by adsorption on the exterior surface under appropriate conditions of temperature and pressure.[3,5,6,12,24−26] The study described in this paper provides the first experimental detection of adsorbed molecules on both the interior and exterior sites on opened SWNTs as well as a method for selective displacement of the internally bound adsorbed molecules. This has been done by working at cryogenic temperatures and observing the adsorbed probe molecule by transmission infrared spectroscopy. It has been found that the vibrational mode observed is red shifted due to interaction with the nanotube surface. The red shift for interior molecules is larger than the shift for exterior adsorbed molecules.

Confinement of CF_4 in pseudo-one-dimensional condensed structures inside the (10,10) nanotube used here does not result in the production of longitudinal optical (LO) and transverse optical (TO) lattice modes observed in 3D clusters of CF_4.

We have employed CF_4(g) as a probe molecule for adsorption on opened single-walled nanotubes.[3,25] CF_4 exhibits an intense triply degenerate asymmetric stretching mode at 1282 cm^{-1}.[27] Its almost spherical shape and polarizability (3.84 $Å^3$) are similar to that of Xe (4.04 $Å^3$), which was used in earlier experiments.[11,18,22,23] The similar properties of CF_4 and Xe make them ideal for interesting adsorbed CF_4 displacement experiments[28] to be reported in this work.

II. Experimental Section

A. Single-Walled Carbon Nanotubes. The SWNTs obtained from Professor R. Smalley's group, Rice University, Houston, TX, were produced by means of the pulsed laser vaporization technique. The raw material was purified by HNO_3/H_2SO_4 treatment.[29] This technique is used to remove foreign carbon impurities and produces oxidized C═O and C−O−C functionalities on the rims and on defect sites in the walls of the SWNTs. These functional groups have been shown to block physical adsorption into the interior of SWNTs, and the groups must be removed by heating to ∼873 K to open the entry ports for adsorption.[23] The tube diameter distribution was centered near that of (10,10) SWNTs with a diameter of 13.6 Å. The length distribution was rather narrow, with the most probable length being 320 nm. The purified SWNTs are observed by SEM to form long bundles. This material was identical to that used in previous studies.[22,23] The purified sample of nanotubes was suspended in dimethylformamide (DMF). About 25 μg of SWNTs was used for this study, which gave a 65 $\mu g/cm^2$ surface density on the sample.

B. Vacuum System and IR Cell. The stainless steel vacuum system is equipped with a 60 L/s turbomolecular pump and a 20 L/s ion pump. The pressure was measured with an ionization gauge (10^{-10}−10^{-4} Torr range) and a capacitance manometer (10^{-3}−10^{3} Torr range). The system base pressure was 10^{-7} Torr after 20 h of baking out at 430−455 K. A UTI 100C quadrupole mass spectrometer was used for leak checking and monitoring of the gas composition in the system.

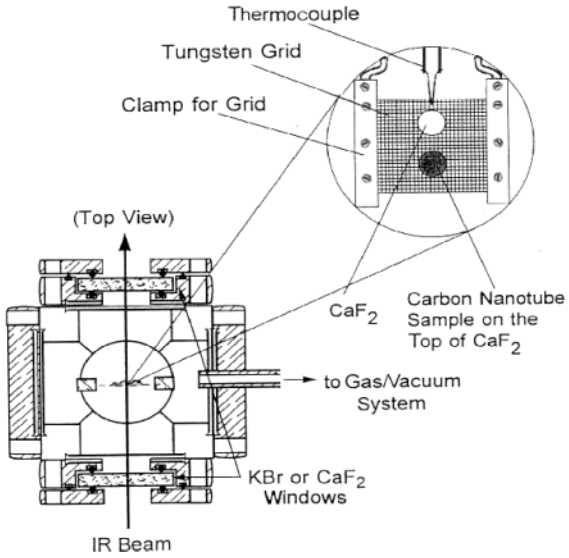

Figure 1. Transmission IR cell cross-section. The cell is moved by means of horizontal and vertical Newport linear activators, allowing precise alignment of the IR beam onto the desired section of the sample grid.

Figure 1 shows the cell used for transmission IR studies. The cell is connected directly to the gas line and was described in detail previously.[30] The SWNT sample is supported on the surface of a CaF_2 spot produced from CaF_2 powder hydraulically pressed at 15000 psi into a tungsten sample support grid. A second CaF_2 spot is used as the reference. The grid is stretched between nickel clamps, which are electrically and thermally connected to copper power leads that enter the cell through a liquid N_2 cooled re-entrant dewar. The grid temperature range is 90 to ∼1500 K. Temperature is measured with a type K thermocouple spot-welded to the top of the grid. Thermal control is accomplished electronically using LabView software, permitting accurate temperature programming as well as temperature stability to ±0.1 K at the temperature of 133 K, the adsorption temperature employed in this work.

When there is an equilibrium pressure of CF_4 in the cell (millitorr range), slight warming of the sample by thermal conduction through the gas phase occurs. This warming effect is automatically compensated by a slight reduction in heating power to the grid, achieving excellent temperature regulation. A temperature gradient in the gas phase results in a slight gas density gradient as one moves vertically along the sample support grid. Thus, subtraction of the gas-phase spectrum (in comparing sample and reference spectra) is not perfect, and a small gas-phase CF_4 IR peak at 1282 cm^{-1} results as well as a small contribution at 1297 cm^{-1} (shoulder) and at 1224 cm^{-1} (shoulder) from CF_4 adsorption on CaF_2.

Condensation of CF_4 occurs on the re-entrant dewar (dewar temperature 77 K) resulting in an equilibrium vapor pressure of CF_4 of 3.3×10^{-2} Torr. This is therefore an upper limit of the gas pressure in this experiment. Lower CF_4 adsorption pressures may be achieved by controlled dosing of small quantities of CF_4 gas into the cooled cell.

C. FTIR Measurements. Transmission IR spectra were measured with a Mattson Research Series FTIR spectrometer controlled from a PC. The spectrometer operates in the mid-infrared spectral region from 500 to 4000 cm^{-1} and uses a wide-band MCT detector. All spectra were recorded at 4 cm^{-1} resolution with 500 scans for averaging. The support grid holding the SWNT sample in the adsorption cell could be accurately positioned horizontally and vertically (to 5 μm) in the IR

(22) Kuznetsova, A.; Yates, J. T., Jr.; Liu, J. Smalley, R. E. *J. Chem. Phys.* **2000**, *112*, 9590.
(23) Kuznetsova, A.; Yates, J. T., Jr.; Simonyan, V. V.; Johnson, J. K.; Huffman, C. B.; Liu, J.; Smalley, R. E. *J. Chem. Phys.* **2001**, *115*, 6691.
(24) Gatica, S. M.; Bojan, M. J.; Stan, G.; Cole, M. W. *J. Chem. Phys.* **2001**, *114*, 3765.
(25) Stan, G.; Bojan, M. J.; Curtarolo, S.; Gatica, S. M.; Cole, M. W. *Phys. Rev. B* **2000**, *62*, 2173.
(26) Kostov, M. K.; Cole, M. W.; Lewis, J. C.; Diep, P.; Johnson, J. K. *Chem. Phys. Lett.* **2000**, *332*, 26.
(27) Fournier, R. P.; Savoie, R.; Bessette, F.; Cabana, A. *J. Chem. Phys.* **1968**, *49*, 1159.
(28) Yang, J.-H.; Clark, L. A.; Ray, G. J.; Kim, Y. J.; Du, H.; Snurr, R. Q. *J. Phys. Chem. B* **2001**, *105*, 4698.
(29) Rinzler, A. G.; Liu, J.; Dai, H.; Nikolayev, P.; Huffman, C. B.; Rodriguez-Macias, F. J.; Boul, P. J.; Lu, A. H.; Heymann, D.; Colbert, D. T.; Lee, R. S.; Fischer, J. E.; Rao, A. M.; Eklund, P. C.; Smalley, R. E. *Appl. Phys.* **1998**, A *67*, 29.
(30) Basu, P.; Ballinger, T. H.; Yates, J. T., Jr. *Rev. Sci. Instrum.* **1988**, *59*, 1321.

sample compartment using computer-controlled drivers. IR spectra were recorded as follows: (1) SWNTs on a CaF_2 support; (2) CaF_2 support; (3) gas phase through the empty grid. In each case the spectra were ratioed to background spectra taken without CF_4 in the system.

Prior to each adsorption experiment a background set of spectra were measured. Upon adsorption of CF_4 a second set of spectra were measured and ratioed to the background. Then appropriate differences were taken to obtain the spectrum of CF_4 adsorbed on the SWNT sample.

D. Controlled Oxidation Using Ozone. The SWNT sample was heated in a vacuum to 873 K to remove the majority of the oxidized surface functionalities produced by the HNO_3/H_2SO_4 purification process and was then subjected to a series of O_3 exposures, followed by annealing to 873 K in vacuum. This cyclic oxidation/annealing procedure has previously been found to open the SWNT caps completely and to enhance the adsorption kinetics into the nanotube interior by opening sites on the nanotube walls and rims.[17−19,22,23] The cyclic procedure causes etching of the SWNT sample, and samples so treated are designated as etched.

High-purity O_3 was prepared and purified in an all-glass generator described previously.[31] We have found that O_3 prepared in this manner will partially decompose upon admission to a stainless steel vacuum system. This effect may be minimized by prolonged passivation of the stainless steel surface with O_3 at ~10 Torr pressure. For the experiment shown here, the O_3 treatment was carried out at room temperature in three stages: (stage 1) 30 min at 8 Torr and 298 K; (stage 2) 19 h at 14.3 Torr and 298 K; (stage 3) 18 h at 15.5 Torr and 298 K. As we will show, initial ozonization produced functional groups at the entrance to the tubes, thus blocking adsorption of CF_4 into the interior of SWNTs in agreement with previous Xe adsorption studies.[18,22] The SWNTs were then opened by removal of the blocking functional groups through heating to 873 K in a vacuum for 30 min. This greatly enhanced the ability of the SWNTs to adsorb CF_4.

E. Xe Displacement Experiment. We employed Xe to preferentially displace adsorbed CF_4 from the nanotube interior. This was done by filling the nanotubes with CF_4 at 3.3×10^{-2} Torr and 133 K. Xe was then added in sequential doses, and the IR spectra of the adsorbed CF_4 were recorded.

F. Gases. CF_4 (99.9% purity) was obtained in a cylinder from Aldrich Chemical Co. and was used without further purification. Xe (99.995%) was obtained from Matheson in a cylinder and was used without further purification.

III. Simulation Methods

A. Vibrational Calculations. The vibrational shifts due to adsorption have been investigated theoretically through quantum calculations using the Gaussian 98 software package.[32] Gas-phase spectra of CF_4 were computed at the levels of LDA theory with the 6-31G basis set. The calculated ν_3 asymmetric stretching mode and ν_4 deformation mode frequencies are 1264 and 573 cm^{-1}, respectively. Quantitative agreement between spectra calculated from LDA and experiment is not expected since LDA does not accurately account for electron correlation, which would account for much of the binding energy. We are also limited in accuracy by the size of the model nanotube and the size of the basis set we were able to use. The LDA calculations of CF_4 adsorbed in the model nanotube gave average frequencies for the ν_3 mode and ν_4 mode of 1246 and 571 cm^{-1}, respectively. We have chosen to use a relatively small basis set (6-31G) to make the CF_4–nanotube calculations tractable. The CF_4–nanotube system was modeled by using a small cluster to represent the nanotube. We used three unit cells of a (9,9) SWNT, split the nanotube in half (along the plane of the nanotube axis), and terminated the dangling bonds with hydrogen atoms. The model nanotube fragment contained 40 carbon and 20 hydrogen atoms. The CF_4 molecule was placed a distance of several angstroms from the concave (inside) surface of the nanotube, and the position of the CF_4 molecule was optimized, holding the atoms in the nanotube fixed. Once the optimized geometry was found, we computed the vibrational spectrum. The optimization and frequency calculations were performed at the LDA/6-31G level of theory.

Table 1. Lennard-Jones Potential Parameters Used in the Simulations

	Xe–Xe	CF_4–CF_4	C–C
σ (Å)	4.1	4.66	3.4
ϵ/k (K)	222.32	134.0	28.0

B. Adsorption Calculations. We have computed the equilibrium amounts of CF_4 and Xe adsorbed on carbon nanotube bundles as a function of Xe partial pressure from molecular simulations. The Grand canonical ensemble (constant μVT) Monte Carlo (GCMC) method.[33] was used to calculate adsorption isotherms. The GCMC algorithm consists of three types of moves, namely, translation of a single molecule, creation of a new molecule in the simulation cell, and deletion of a molecule. Moves were attempted randomly with probability 0.2 for translation and 0.4 each for creation and deletion. Simulations were typically equilibrated for two million moves, followed by data taken for one million moves. The maximum displacement step size was adjusted during equilibration to achieve approximately a 40% acceptance ratio for translations. We have used the Lennard-Jones (LJ) potential to account for all fluid−fluid and fluid−solid interactions. Parameters for Xe were taken from the literature.[34] The CF_4 molecule was treated as a single spherical particle. The LJ parameters were derived from viscosity data[35] and were previously used in molecular simulations of diffusion in zeolites.[36] The carbon parameters were taken from Steele.[37] Lorentz−Berthelot combining rules were used for the cross-interactions. The LJ potential parameters are given in Table 1, where σ is the molecule diameter in angstroms and ϵ is the potential well depth such that ϵ/k is in units of kelvin, where k is the Boltzmann constant. The use of classical potentials to model the nanotube−fluid interactions precludes the modeling of electronic effects, such as the differences between metallic and nonmetallic nanotubes.

Three different nanotube bundles were considered in this work. Two bundles were constructed by randomly placing nanotubes of various diameters in a box and then optimizing the spacing between the nanotubes as described by Simonyan and Johnson.[38] Each of these two bundles contained 18 nanotubes. The third bundle was a perfect 3×3 array of (10,10) nanotubes. The numbers of each type of nanotube in each bundle are given in Table 2. Using the nomenclature of Table 2, bundles 1 and 2 are representative of heterogeneous bundles, i.e., bundles with a heterogeneous distribution of nanotube diameters. Bundle 3 is a homogeneous bundle since all nanotubes have the same diameter.

(31) Zhukov, V.; Popova, I.; Yates, J. T., Jr. *J. Vac. Sci. Technol., A* **2000**, *18*, 992. See also Yates, J. T., Jr. *Experimental Innovations in Surface Science*; Springer-Verlag and American Institute of Physics: New York, 1998.
(32) Gaussian 98, Revision A.11: Frisch, M. J.; Trucks, G. W.; Schlegel, H. B.; Scuseria, G. E.; Robb, M. A.; Cheeseman, J. R.; Zakrzewski, V. G.; Montgomery, J. A., Jr.; Stratmann, R. E.; Burant, J. C.; Dapprich, S.; Millam, J. M.; Daniels, A. D.; Kudin, K. N.; Strain, M. C.; Farkas, O.; Tomasi, J.; Barone, V.; Cossi, M.; Cammi, R.; Mennucci, B.; Pomelli, C.; Adamo, C.; Clifford, S.; Ochterski, J.; Petersson, G. A.; Ayala, P. Y.; Cui, Q.; Morokuma, K.; Salvador, P.; Dannenberg, J. J.; Malick, D. K.; Rabuck, A. D.; Raghavachari, K.; Foresman, J. B.; Cioslowski, J.; Ortiz, J. V.; Baboul, A. G.; Stefanov, B. B.; Liu, G.; Liashenko, A.; Piskorz, P.; Komaromi, I.; Gomperts, R.; Martin, R. L.; Fox, D. J.; Keith, T.; Al-Laham, M. A.; Peng, C. Y.; Nanayakkara, A.; Challacombe, M.; Gill, P. M. W.; Johnson, B.; Chen, W.; Wong, M. W.; Andres, J. L.; Gonzalez, C.; Head-Gordon, M.; Replogle, E. S.; Pople, J. A., Gaussian, Inc., Pittsburgh, PA, 2001.
(33) *Computer Simulation of Liquids*; Allen, M. P., Tildesley, D. J., Eds.; Clarendon: Oxford, 1987.
(34) *Statistical Mechanics for Thermophysical Property Calculations*; Rowley, R. L., Ed.; Prentice Hall: Englewood Cliffs, NJ, 1994.
(35) *The Properties of Gases and Liquids*, 5th ed.; Poling, B. E., Prausnitz, J. M., O'Connell, J. P., Eds.; McGraw-Hill: New York, 2001.
(36) Snurr, R. Q.; Kärger, J. *J. Phys. Chem. B* **1997**, *101*, 6469.
(37) Skoulidas, A. I.; Sholl, D. S. *J. Phys. Chem. B* **2001**, *105*, 3151. Steele, W. A. *Surf. Sci.* **1973**, *36*, 317.
(38) Simonyan, V. V.; Johnson, J. K. Manuscript in preparation.

Table 2. Number and Types of Nanotubes Used in the Three Different Bundles

bundle	no. of (8,8) tubes	no. of (9,9) tubes	no. of (10,10) tubes	no. of (11,11) tubes	no. of (12,12) tubes	av nanotube diameter (Å)
1	2	2	10	2	2	13.56
2	4	10	2	2	0	12.35
3	0	0	9	0	0	13.56

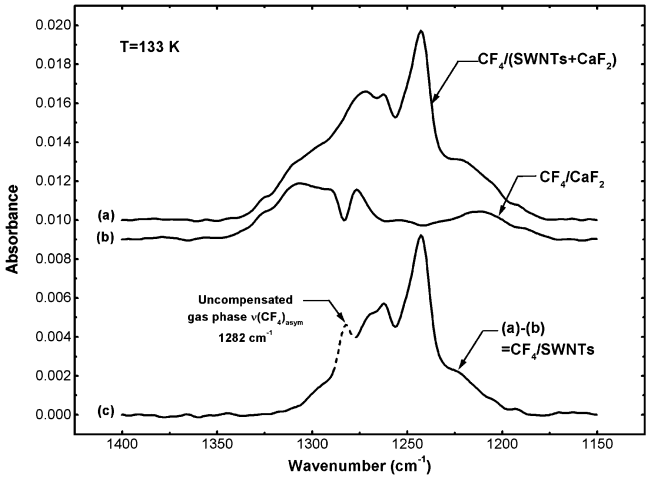

Figure 2. Procedure for spectral subtraction for CF_4 adsorbed at 133 K and $3.3 \cdot 10^{-2}$ Torr.

Experimentally produced nanotubes are heterogeneous. Comparison of simulations on these two classes of bundles will serve to characterize any qualitative differences between adsorption on homogeneous and heterogeneous bundles. Smoothed potentials were used for the nanotubes in the bundles to increase the simulation efficiency. See ref 11 for details of the smoothing procedure. We have found that smoothing the potential has no effect on the adsorption isotherms.[11] The nanotubes in the simulation cell were all aligned in the *z* direction, and the lengths of the nanotubes were about 60 Å. The bundle was placed in a parallelepiped simulation cell that was 200 Å on a side in the *x* and *y* directions. Periodic boundary conditions were applied in all directions, and the potential cutoff was set to 25 Å. The size of the cell in the *x* and *y* directions was large enough so that the bundle was isolated (no periodic image interactions).

IV. Results

A. Development of the CF_4 IR Spectrum upon SWNT Etching by O_3. Figure 2 shows a typical set of IR spectra obtained in these measurements and the results of taking appropriate differences to derive the IR spectrum of CF_4 adsorbed on the SWNT sample. The CaF_2 support exhibits a significant contribution to the composite IR spectrum due to CF_4 adsorption on its surface, as seen in spectrum b. Additional IR absorbance due to CF_4 is observed for the SWNT sample, supported on CaF_2, as shown in spectrum a. Subtraction leads to spectrum c, where contributions from adsorbed CF_4 on the SWNT sample are observed, along with small features due to incompletely compensated gas-phase CF_4. The prominent uncompensated gas-phase spectral feature is shown as a dashed peak centered at 1282 cm^{-1}.

Figure 3 shows the infrared spectrum of adsorbed CF_4 as increasing amounts of etching take place through repeated exposures to O_3, followed by heating. Three etch cycles are presented. As the etching proceeds, enhanced IR intensity due to adsorbed CF_4 is observed to occur at frequencies below 1275 cm^{-1}.

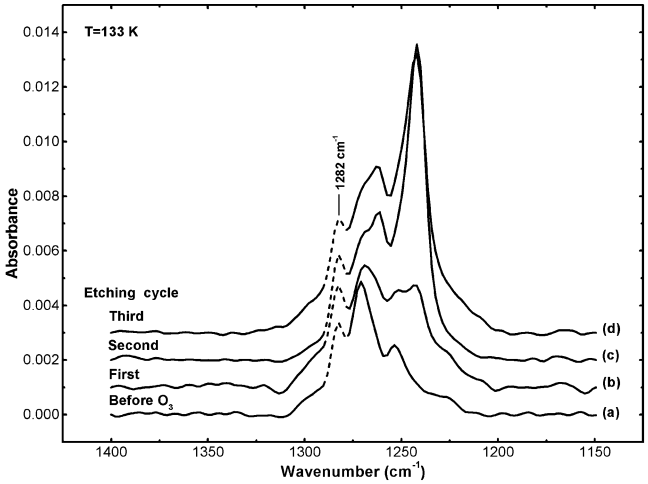

Figure 3. Development of CF_4 IR spectra during cycles of O_3-induced oxidation followed by heating to 873 K for 30 min in a vacuum. $P_{CF_4} = 3.3 \times 10^{-2}$ Torr.

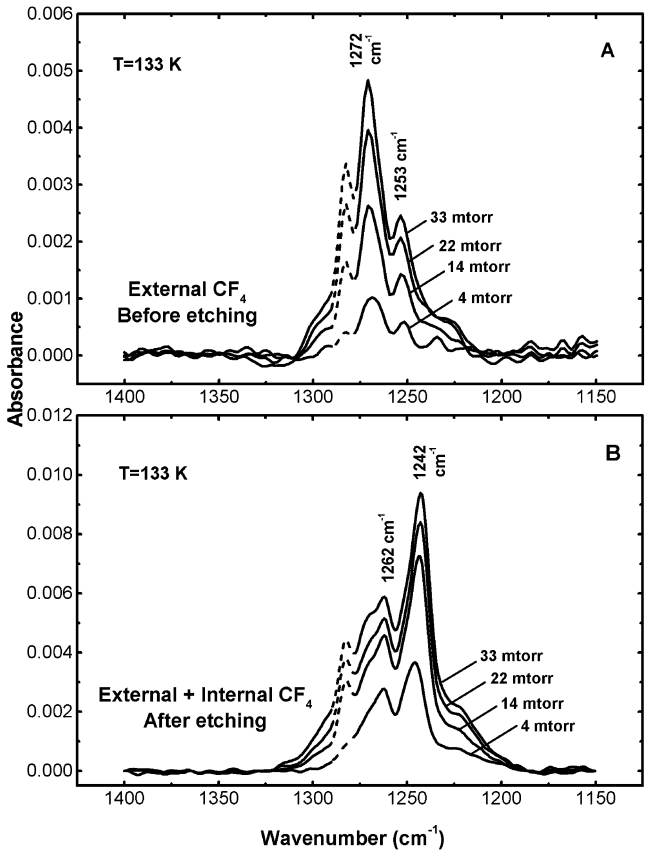

Figure 4. Development of CF_4 IR spectra for (A) external sites and (B) external plus internal sites.

Figure 4 shows a comparison of the development of the IR spectrum of CF_4 for increasing coverage on the SWNT sample before etching by O_3 and after three cycles of etching. Note that the absorbance scales differ by a factor of 2 for the spectral presentations. The spectra show the effects of increasing equilibrium pressures of CF_4, established at a sample temperature of 133 K. The spectra shown in Figure 4A for the unetched SWNTs contain only two prominent spectral features for adsorbed CF_4 at 1272 and 1253 cm^{-1}. For the etched SWNT sample (Figure 4B), in addition to the spectral features observed in Figure 4A, an additional pair of absorption bands are observed

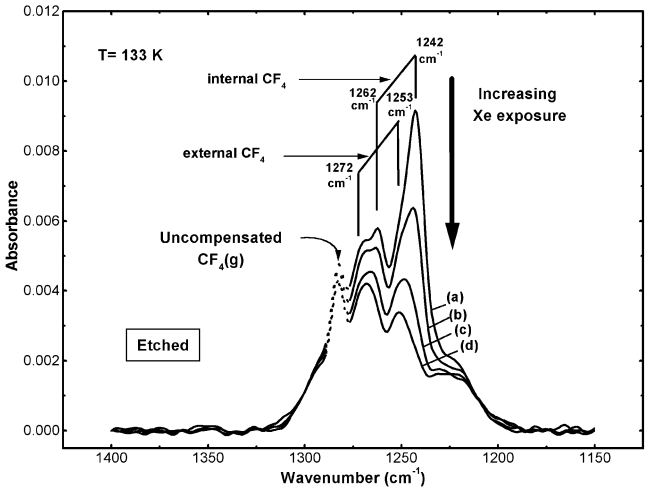

Figure 5. Xe displacement of adsorbed CF_4. The equilibrium Xe pressure was less than 10^{-3} Torr for (a)−(d). The equilibrium $P_{CF_4} = 3.3 \times 10^{-2}$ Torr for all spectra.

at 1262 and 1242 cm^{-1}. As will be discussed later, the pairs of bands observed at different frequencies for the unetched and etched nanotubes are due to the Fermi resonance of the strong infrared-active ν_3 mode and the first overtone of the ν_4 mode, designated $2\nu_4$.

B. Displacement of Adsorbed CF_4 by Xe. The resolution of the overlapping CF_4 spectral features has been experimentally confirmed through the displacement of CF_4 by Xe. Figure 5 shows a high-coverage spectrum of CF_4 obtained for the etched SWNT sample. Exposure to Xe at 133 K results in the selective disappearance of two IR bands together at 1262 and 1242 cm^{-1}. In contrast, the species responsible for the two bands at 1272 and 1253 cm^{-1} either are not displaced or are more slowly displaced compared to the former band pair. We assign the two bands at 1262 and 1242 cm^{-1} to CF_4 adsorbed in the interior of the etched SWNT sample, and the two bands at 1272 and 1253 cm^{-1} to CF_4 species adsorbed externally on the outer SWNT surface. By varying the sequence of Xe and CF_4 adsorption, it was found that the spectra represent identical equilibrium conditions achieved by gas adsorption in either sequence.

V. Discussion

A. Absence of LO−TO Splitting in IR Spectra of CF_4 on SWNTs. The ν_3 mode in CF_4 has an exceptionally high infrared intensity.[27] This gives rise to a strong transition dipole−transition dipole coupling between ν_3 modes of different CF_4 molecules. As a result LO−TO splitting appears in the infrared spectra at high volumetric concentrations of oscillators. The splitting is strongly dependent on the arrangement of the oscillators. We have not observed LO−TO splitting in this work, implying that the concentration of CF_4 molecules inside and on the exterior of the SWNT sample is not sufficiently bulklike to promote lattice mode production.

Figure 6A shows the LO−TO mode splitting evolution in the Raman spectra of CF_4 in an Ar matrix at 84.5 K taken as an example from the work of P. Nextoux et al.[39] More examples of LO−TO splitting in the vibrational spectra of CF_4 in the condensed phase can be found elsewhere.[40−45] At a very low

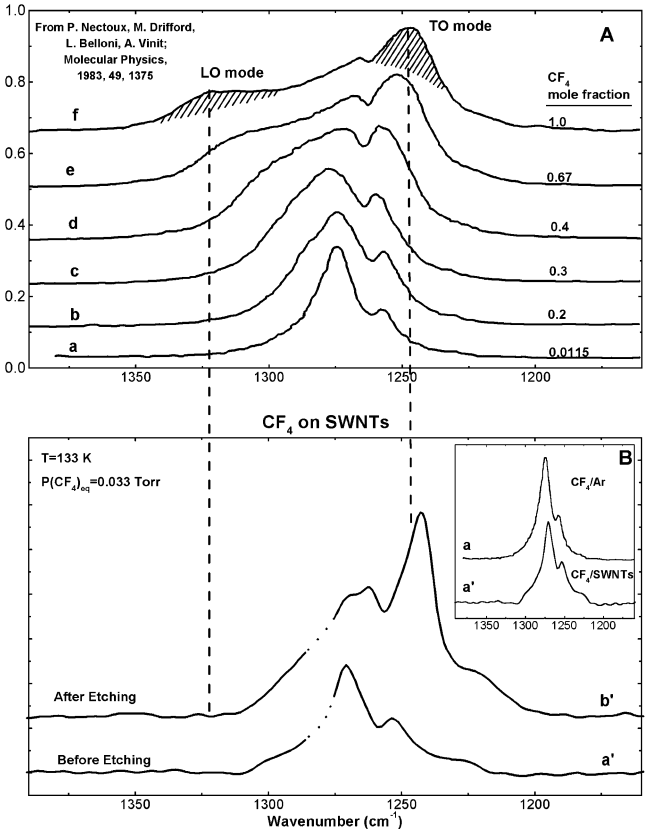

Figure 6. (A) LO−TO splitting evolution in Raman spectra of CF_4 in an Ar matrix at 84.5 K with increasing concentration. (B) Infrared spectra of CF_4 adsorbed at 133 K and 0.033 Torr on unetched and etched SWNTs.

concentration of CF_4, spectrum a, two peaks at 1272 and 1257 cm^{-1} caused by the Fermi resonance interaction of ν_3 and $2\nu_4$ are observed. The LO−TO splitting is very small in this case and reported to be 1.4 cm^{-1}. In pure condensed CF_4, spectrum f, LO−TO splitting reaches 75.0 cm^{-1} with the LO band at 1320 cm^{-1} and TO band at 1245 cm^{-1}.

Figure 6B shows the spectrum of CF_4 adsorbed on unetched and etched nanotubes. The close similarity of the IR spectrum of CF_4 adsorbed on SWNTs before etching to the Raman spectra of CF_4 in an Ar matrix at the lowest concentration (see the inset in Figure 6B) implies that there is a similarly negligible amount of LO−TO splitting in the spectra of CF_4 adsorbed on the external surface of nanotubes at these conditions. No evidence for LO or TO modes can be seen.

As the nanotubes are etched the internal surface becomes accessible for adsorption. The IR spectra of CF_4 adsorbed on the etched SWNTs (Figure 6B, upper spectrum) contain features from both the external and the internal CF_4. Although the amount of CF_4 adsorbed has increased somewhat compared to that of unetched nanotubes, the LO mode is not seen and the peak at 1242 cm^{-1} cannot be considered to be the TO band because of its sharpness.

(39) Nextoux, P.; Drifford, M.; Belloni, L.; Vinit, A. *Mol. Phys.* **1983**, *49*, 1375.
(40) Rowland, B.; Kadagathur, N. S.; Devlin, J. P. *J. Chem. Phys.* **1995**, *102*, 13.
(41) Buch, V.; Delzeit, L.; Blackledge, C.; Devlin, J. P. *J. Phys. Chem.* **1996**, *100*, 3732.
(42) Delzeit, L.; Delvin, M. S.; Rowland, B.; Delvin, J. P.; Buch, V. *J. Phys. Chem.* **1996**, *100*, 10076.
(43) Jones, L. H.; Swanson, B. I. *J. Phys. Chem.* **1991**, *95*, 2701.
(44) Gilbert, M.; Drifford, M. *J. Chem. Phys.* **1977**, *66*, 3205.
(45) Daly, F. P.; Hopkins, A. G.; Brown, C. W. *Spectrochim. Acta* **1974**, *30A*, 2159.

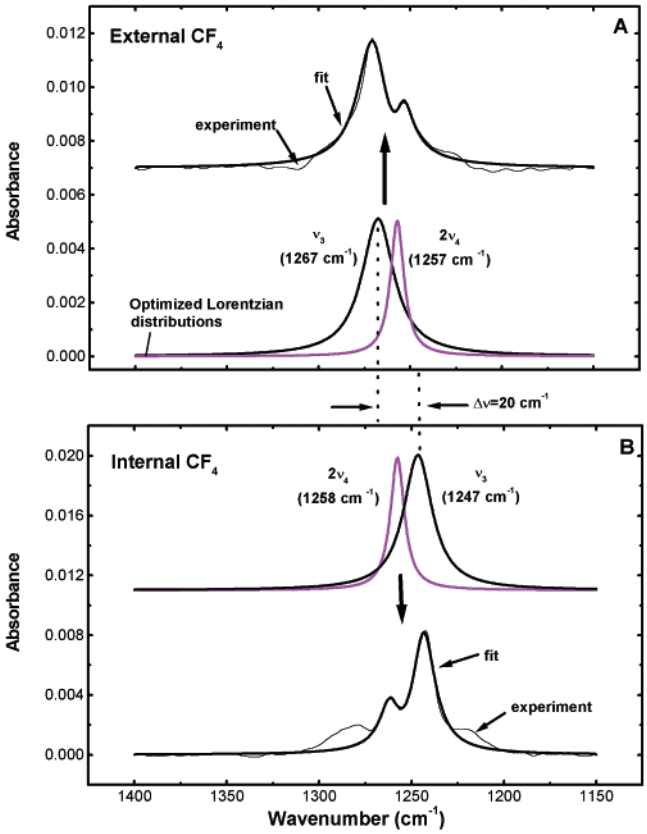

Figure 7. Fermi resonance interaction of the fundamental ν_3 mode with the $2\nu_4$ mode for external and internal CF_4 species on SWNTs. The fit was numerically calculated from the Lorentzian distributions, which were iteratively optimized for the fit to match the experimental spectrum. The interaction strength parameter was allowed to vary slightly to fit the data. It is 6.3 and 7.6 cm^{-1} for unetched (A) and etched (B) samples, respectively.

Thus, the mean size of adsorbed CF_4 ensembles on the inner and outer surfaces of the SWNTs must be too small to produce the LO−TO modes characteristic of the condensed phase.

B. Spectra of CF_4 Adsorbed on SWNTs. In vibrational spectroscopy, perturbations between a fundamental and an overtone are frequently encountered, and are known as Fermi resonances.[46] In the case of the CF_4 molecule, the Fermi resonance between the ν_3 mode and the first overtone of the ν_4 mode ($2\nu_4$) has been observed in a number of studies.[47−51] As a result of the interaction the overtone, usually very weak, borrows intensity from the fundamental band and becomes visible, and at the same time the two bands are shifted further apart. Thus, the presence of a Fermi resonance complicates the appearance of the spectrum, so it is often useful to extract the "unperturbed" positions and intensities of the peaks. This was done in the present study in a way similar to that employed in ref 46. For the spectra of CF_4 on etched and unetched nanotubes, Lorentzian-shaped profiles of ν_3 and $2\nu_4$ were found that upon numerically calculating the Fermi resonance interaction gave the best fits to the spectra observed.

Figure 7A shows the spectrum of CF_4 on unetched nanotubes, which corresponds to CF_4 adsorbed on the outer surface of nanotubes, and the Lorentzian profiles found for the ν_3 and $2\nu_4$ energy level distributions. The fit calculated from these two distributions approximates the experimental data well. The presence of the $2\nu_4$ energy level redistributes the intensity of ν_3 in the spectrum, creating an additional feature at 1253 cm^{-1} and a "hole" (sometimes referred to as the Evans hole in the literature) at 1257 cm^{-1}. Note that, for CF_4 molecules bound to the SWNTs exterior, the ν_3 level is located to the higher frequency side of $2\nu_4$.

CF_4 on etched nanotubes should be adsorbed on both the outer surface and the inner surface, made accessible by the etching, whereas the spectrum for unetched nanotubes only contains the contribution from the outer CF_4. To find the spectrum of only the inner CF_4, one thus needs to subtract the spectrum for the unetched nanotubes from the spectrum for the etched nanotubes. As some of the SWNT surface is destroyed in the process of etching with ozone, the spectrum from the unetched nanotubes has to be multiplied by a coefficient smaller than 1 before the subtraction is carried out. We used a value of 0.75, chosen on the basis of the goodness of the fit to the resulting spectrum. It corresponds to the destruction of 25% of the outer surface during ozonation. Figure 7B shows the spectrum of CF_4 adsorbed on the inner surface of nanotubes resulting from this subtraction and the Lorentzian distributions of ν_3 and $2\nu_4$ that give the best fit to the data. The most striking difference when compared to the external CF_4 distributions (Figure 7A, bottom) is that ν_3 shifts by 20 cm^{-1} to the red (now ν_3 is to the lower energy side of $2\nu_4$), whereas $2\nu_4$ does not change its position. The reason for the shift of ν_3 is the stronger interaction of the molecule with the surface when it is adsorbed in the interior of the nanotube. The LDA calculation also shows that the ν_3 band is much more prone to shift when the molecule's environment changes than the $2\nu_4$ mode (as judged from the ν_4 fundamental). The calculation indicates that, for the CF_4 molecule adsorbed in the interior of the nanotube, the ν_3 mode shifts by about −20 cm^{-1} compared to that in the gas phase, whereas the shift for ν_4 is only −2 cm^{-1} corresponding to a $2\nu_4$ shift of about −4 cm^{-1}.

This analysis of the experimental spectra shows that the shift for the ν_3 mode of CF_4 compared to gas-phase CF_4 is −15 cm^{-1} for CF_4 molecules bound to the nanotube outer surface and −35 cm^{-1} for CF_4 molecules bound in the interior.

Figure 8 shows the addition of the fits for the external and internal CF_4 spectra, resulting in a fit for the total composite spectrum of CF_4 adsorbed on etched nanotubes. The coefficient of 0.75 is employed during addition.

The shift of the ν_3 mode to lower wavenumbers is in accordance with the red shift often observed for physically adsorbed species and for species bound inside inert matrixes. The band associated with the smaller ν_3 red shift is assigned to externally bound CF_4 molecules on this basis as well as on the basis of comparison of CF_4 spectra on etched and unetched nanotubes, and the band associated with the larger wavenumber shift is assigned to internally bound CF_4, where the interaction would be expected to be larger.

C. Modeling of Xe Displacement of Adsorbed CF_4 from SWNTs. The displacement of CF_4 by Xe confirms the presence of four IR bands for the adsorbed CF_4 species present on both the exterior and interior sites. It is seen in Figure 5 that Xe preferentially displaces internal CF_4 species, causing the bands

(46) Scherer, J. R. *Adv. Infrared Raman Spectrosc.* **1978**, *5*, 149−216.
(47) Evans, J. C.; Wright, N. *Spectrochim. Acta* **1960**, *16*, 352.
(48) Evans, J. C. *Spectrochim. Acta* **1960**, *16*, 994.
(49) Bertie, J.; Devlin, J. P. *J. Chem. Phys.* **1983**, *79* (4), 2092.
(50) Devlin, J. P.; Wooldridge, P. J.; Ritzhaupt, G. *J. Chem. Phys.* **1986**, *84* (11), 6095.
(51) Scherer, J. R.; Go, M. K.; Kint, S. *J. Phys. Chem.* **1973**, *77* (17), 2108.

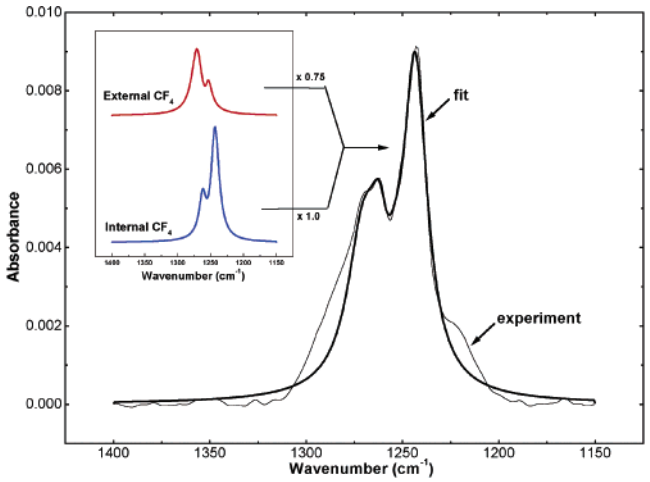

Figure 8. Simulation of combined external and internal CF_4 spectra on SWNTs.

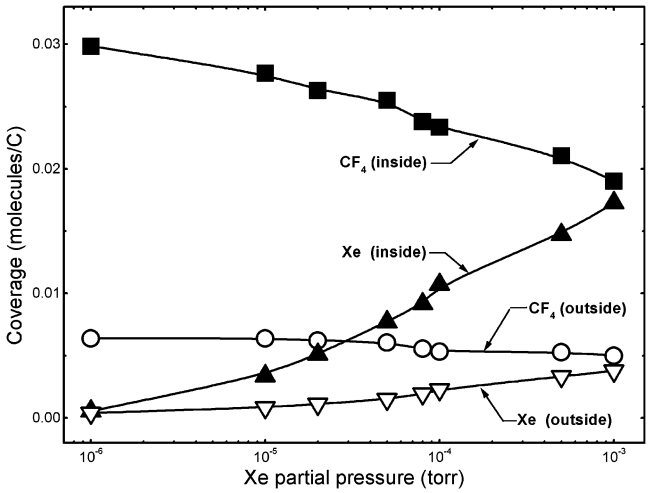

Figure 9. Simulated equilibrium adsorption uptake of CF_4 and Xe (per carbon atom) on heterogeneous nanotube bundle 1 (see Table 2) at 133 K as a function of Xe partial pressure. The CF_4 pressure is held constant at 3.3×10^{-2} Torr. Squares (circles) represent the loading of CF_4 molecules inside (outside) the nanotubes and up triangles (down triangles) represent Xe adsorption inside (outside) the nanotubes. Lines are drawn to guide the eye. The estimated statistical errors are on the order of the symbol sizes.

at 1262 and 1242 cm^{-1} to disappear first as the Xe coverage is increased. The displacement experiments probe the thermodynamic factors responsible for Xe−CF_4 site exchange under equilibrium conditions, since similar infrared spectra are observed for either order of adsorption of CF_4 and Xe. We know that Xe is thermodynamically favored as an internally bound species compared to CF_4, causing preferential CF_4 displacement by Xe from the SWNT interior. We have performed molecular modeling of CF_4 and Xe coadsorption to observe whether preferential CF_4 displacement occurs for the internally bound CF_4 compared to externally bound CF_4. Classical GCMC simulations were performed at 133 K, a constant partial pressure of CF_4 of 3.3×10^{-2} Torr, and various values of Xe partial pressure. Simulations were performed on each of the three model bundles described in Table 2. The results from two simulations on heterogeneous and homogeneous bundles are shown in Figures 9 and 10, respectively. Simulations on the three different types of bundles are qualitatively similar. In each case Xe begins to adsorb inside the nanotubes, displacing CF_4, at pressures

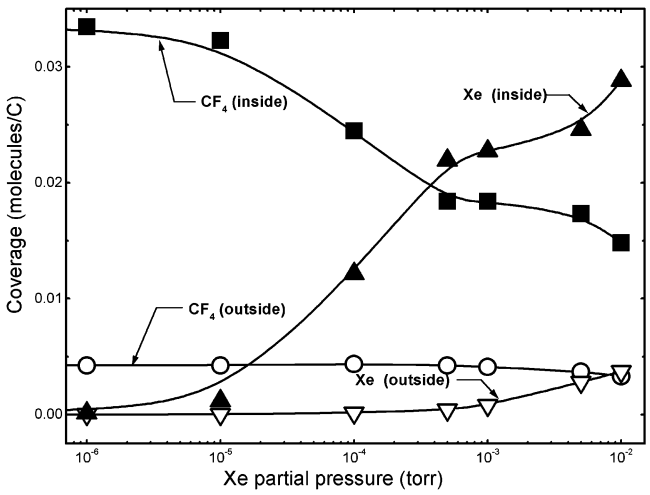

Figure 10. Simulated equilibrium coverage of CF_4 and Xe (expressed per carbon atom) on homogeneous nanotube bundle 3 (see Table 2) at 133 K as a function of Xe partial pressure. The CF_4 pressure is held constant at 3.3×10^{-2} Torr. The symbols are the same as in Figure 9. The lines are drawn to guide the eye.

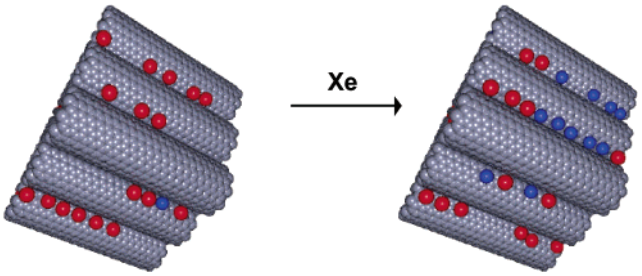

Figure 11. Simulation snapshots for CF_4-Xe coadsorption on the external groove sites at a Xe partial pressure of 10^{-3} Torr (left) and 5×10^{-3} Torr (right). In both cases the CF_4 pressure is 3.3×10^{-2} Torr. Note that the number of Xe atoms (blue) increases dramatically with increasing Xe partial pressure, while the number of CF_4 molecules (red) decreases only slightly.

below where there is appreciable Xe adsorption in the grooves on the external surface of the nanotubes. The partial pressure at which Xe begins to displace internal CF_4 is about 10^{-5} Torr. Xenon starts to adsorb on the outside of the nanotubes at about 10^{-4} Torr for the heterogeneous bundle and about 10^{-3} Torr for the homogeneous bundle. It is interesting to note that, even after Xe begins to adsorb on the outside of the nanotubes, very little CF_4 is displaced by the Xe, even at the highest Xe partial pressure simulated (10^{-2} Torr). This observation agrees with the experimental results showing that the CF_4 modes associated with adsorption inside the nanotube disappear in a facile manner, while the IR peaks for external adsorption are not substantially attenuated by Xe adsorption. The reason for this can be easily seen by observing snapshots of the simulation. Figure 11 shows snapshots for adsorption on exterior sites of bundle 3 at Xe partial pressures of 10^{-3} (left) and 5×10^{-3} (right) Torr, both with a CF_4 partial pressure of 3.3×10^{-2} Torr. Note that at the lower Xe partial pressure there are a number of CF_4 molecules (shown in red) but only one Xe atom (blue). Note also that CF_4 does not fill all the available external sites at this pressure. Hence, at the higher pressure (right) we observe a dramatic increase in the concentration of Xe atoms in the groove sites, while the number of CF_4 molecules remains almost constant. The first Xe atoms to adsorb onto the external sites simply occupy empty sites rather than replacing CF_4 molecules. At

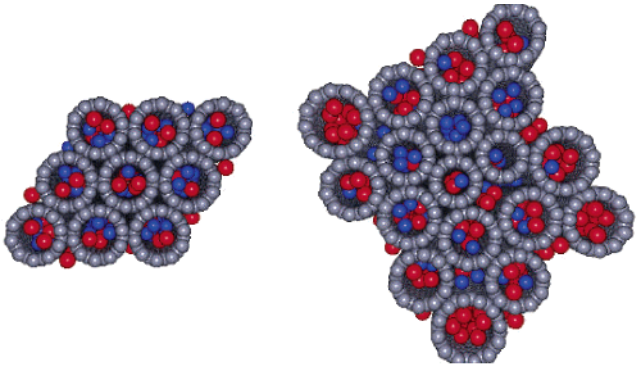

Figure 12. Simulation snapshots for CF_4-Xe coadsorption on homogeneous bundles (left) and on heterogeneous bundles (right). Note that the interstitial channels in the homogeneous bundle are too small to allow adsorption of either Xe or CF_4. The interstitial channels in heterogeneous bundles, such as bundle 1 from Table 2 shown here (right), have some larger interstitial channels that allow adsorption of Xe and CF_4.

pressures higher than those sampled experimentally, Xe does displace CF_4 on the external sites. This explains why external CF_4 species responsible for the bands at 1272 and 1253 cm^{-1} persist at all experimental Xe doses.

Molecular simulations show that Xe and CF_4 only adsorb inside the nanotubes and on the external groove of the perfectly packed homogeneous bundles (bundle 3). The interstitial channels in homogeneous bundles of (10,10) nanotubes are too small to allow adsorption of either gas. However, the heterogeneous bundles do not pack perfectly and hence have a few larger interstitial sites for gas adsorption. Simulation snapshots from homogeneous and heterogeneous bundles are shown in Figure 12. Most of the interstitial channels in the heterogeneous bundle (left) are too small to accommodate adsorption of either Xe or CF_4. However, there are a few interstices that are large enough to facilitate Xe, but not CF_4, adsorption and other channels that are large enough to accommodate either molecule. This explains why the heterogeneous bundles (Figure 9) exhibit external Xe adsorption at lower pressures than the homogeneous bundles (Figure 10). Adsorption in the interstitial channels is counted as external site adsorption so that the upturn in external Xe site adsorption shown in Figure 10 is a result of Xe inside the interstitial channels. We expect that the nanotube bundles studied experimentally behave more like the heterogeneous bundles than the perfectly packed bundles, giving rise to some interstitial adsorption.

VI. Summary

The following results have been obtained in our study of CF_4 adsorption on unetched SWNTs and etched SWNTs.

(1) The adsorption of CF_4 on SWNTs at 133 K occurs on two adsorption sites: internal and external. On closed SWNTs, CF_4 adsorbs only on the external sites, whereas on opened SWNTs, CF_4 adsorbs on both external and internal sites.

(2) Adsorbed CF_4 on external sites of SWNTs manifests itself by two IR bands, at 1272 and 1253 cm^{-1}. CF_4 adsorbed on internal sites exhibits two bands at 1262 and 1242 cm^{-1}. The presence of two bands in both cases results from the Fermi resonance of the strong infrared-active ν_3 fundamental with the first overtone of the ν_4 mode.

(3) The larger shift from the gas-phase frequency of the ν_3 mode of internal CF_4 (shift -35 cm^{-1}, -2.7%) compared to the external CF_4 (shift -15 cm^{-1}, -1.2%) is due to the stronger interaction of CF_4 with the interior walls of SWNTs.

(4) Xe preferentially displaces CF_4 adsorbed inside SWNTs as observed both experimentally and in equilibrium simulations.

(5) The confinement of CF_4 inside the (10,10) single-walled nanotube in pseudo-one-dimensional structures does not result in production of LO and TO lattice modes characteristic of large 3D ensembles of CF_4 in crystallized CF_4.

Acknowledgment. We gratefully acknowledge the Army Research Office for the support of this work. We also acknowledge support from Dr. Chris Karwacki at the Aberdeen Proving Ground. We thank Wei Shi for helpful discussions. We also gratefully acknowledge the suggestions of an anonymous reviewer regarding the spectroscopic interpretation of our results. Simulations were performed at the University of Pittsburgh's Center for Molecular and Materials Simulations.

JA020949G